Hybrid density functional theory insight into the stability and microscopic properties of Bi-doped $LiNbO_3$: Lone electron pair effect

Lili Li, Yanlu Li,* and Xian Zhao†

State Key Laboratory of Crystal Materials, Shandong University, Jinan 250100, China

(Received 1 June 2017; revised manuscript received 26 July 2017; published 11 September 2017)

It has recently been reported that Bi-doped $LiNbO_3$ exhibits more excellent photorefractive properties than the traditional Fe doping. Bi-induced structural and physical properties remain unverified by either experiment or theory, however. Thus, here the basic characteristics of Bi-doped $LiNbO_3$, such as the preferable Bi doping site, local lattice distortion, and the effect of Bi doping on the electronic structure and optical properties, are investigated by density functional theory with a hybrid functional. In particular, we focus on the effect of a Bi lone electron pair on the structural distortion and polaronic behavior of $LiNbO_3$. The calculated results show that Bi substitutional Li in its +4 charge state (Bi_{Li}^{4+}) and Bi substitutional Nb in its neutral state (Bi_{Nb}^{0}) are energetically preferable in the majority of $LiNbO_3$ samples. The incorporation of Bi could form a small bound electron polaron in $LiNbO_3$. The strongly polarized localization of the Bi $6s^2$ lone electron pair around the Bi center dominantly contributes to the large local lattice relaxation and the huge energy gain of Bi_{Li}^{2+} that result in the negative U effect. A new $Bi_{Li}^{4+/2+}$ photorefractive center that is 2.2 eV deeper than the intrinsic $Nb_{Li}^{4+/2+}$ photorefractive center is introduced by Bi doping.

DOI: 10.1103/PhysRevB.96.115118

I. INTRODUCTION

$LiNbO_3$, one of the multifunctional optical materials with excellent photorefractive, electro-optical, and nonlinear optical properties, has been widely used for optical data storage [1] by holographic recording, optical modulators, and phase-conjugated mirrors [2,3]. During the past decades, there have been a large number of studies on the photorefractivity of $LiNbO_3$ since the homogeneous crystal is available and exhibits a strong photorefractive effect at room temperature [4,5]. Specifically, it is well demonstrated that the photorefractivity of $LiNbO_3$ can be modified by controlling extrinsic doping and intrinsic defects in crystals [6,7]. It is reported that $LiNbO_3$ doped with Mg [8], Zn [9], etc., could greatly increase the resistance against photorefractive damage, while dopants such as Fe [10,11] and Cu [11] are introduced to enhance the photorefractive properties of $LiNbO_3$ by trapping d electrons in defect levels. Therefore, dopants play an important role in controlling the photorefractive properties of $LiNbO_3$.

Many experiments have shown that Bi always brings out excellent physical and chemical properties in some crystals due to its lone electron pair. For example, Bi mainly contributes to the improved nonlinear optical characteristics of $Cd_4BiB(BO_3)_3$ [12] due to the stereochemically active Bi^{3+} ($6s^2$) lone electron pair. Also, the excellent ferroelectricity and electro-optical properties of Bi-containing perovskites [13] come from the high polarizability of the lone electron pair associated with the Bi^{3+} ion. It is well known that the lone electron pair often exhibits a negative polar character with high charge density, which will modify its nearby local atomic configuration by the strong repulsion between the electrons. The Bi dopant is also expected to bring out some particular optical properties, especially photorefractive properties, in $LiNbO_3$ due to the effect of the lone electron pair.

Recently, Kong *et al.* [14] reported the successful growth of Bi-doped $LiNbO_3$ (Bi:$LiNbO_3$) and its enhanced photorefractive performance with respect to the famous Fe-doped $LiNbO_3$, such as acceleration of the photorefractive response and increased photorefractive sensitivity, which are strongly influenced by, or even depend on, the new photorefractive center owing to Bi dopants. It is also pointed out [14] that Bi:$LiNbO_3$ might exhibit a threshold behavior—a threshold near 1.0 mol% corresponding to the lattice occupation change of Bi^{3+} from Li to Nb site, which is similar to the lattice occupation for other dopants such as Mg, Zn, and Fe in $LiNbO_3$ [15–17]. As illustrated in many experimental papers [8,18,19], lattice Li sites always include both Nb_{Li} sites and normal Li sites that have absolutely the same lattice environment and configuration. The incorporation site preference of Bi from both experiment and theory is not clear. Otherwise, there has been little in the experimental and theoretical literature on the Bi lattice occupation and the related properties of Bi:$LiNbO_3$. It is of great importance to understand the most basic characteristics of Bi doping, especially on the carrier self-trapping action, which will help us to better understand the origin and mechanism of the enhanced photorefractive properties of Bi:$LiNbO_3$. More recently, it became clear that the photorefractive process in $LiNbO_3$ refers to the photoexcitation of the carrier from the trapped states to the conduction band (CB) and the recapture of the carrier in the CB by the trapped states. During this process, the charge transport in $LiNbO_3$ can be described as small polarons [20,21] in which the charge and the lattice deformation can move as a whole by thermally activated hopping [22,23], and eventually be trapped by crystal defects and impurities. In Bi:$LiNbO_3$, the charge distribution and lattice distortion of small polarons might be influenced by the lone electron pair, which may bring out interesting electronic and optical properties of $LiNbO_3$. These basic understanding of Bi doping, though of great importance, is quite limited at present. Theory supplies an effective way to direct and investigate in detail the microscopic behavior of Bi:$LiNbO_3$, which is highly complementary to experimental

*liyanlu@sdu.edu.cn
†xianzhao@sdu.edu.cn

studies. Particularly, we emphasize studying the effect of the Bi lone electron pair on the electronic and photorefractive properties of $LiNbO_3$ with respect to the other photorefractive ions.

In this work, the lattice deformation, energetics, and carrier trapping behavior of Bi:$LiNbO_3$ have been investigated by using the state-of-the-art first-principles approach based on density functional theory (DFT) [24,25]. The normally used (semi)local functional always underestimates the band gaps of semiconductors, which severely affects the predictive power of the approximation when applied to defect levels, particularly severely in cases of strong correlations such as occur in the highly localized Nb d states [26,27]. Thus the Hyde-Scuseria-Ernzerhof (HSE06) hybrid functional [28,29] is used to improve the description of the electronic structures and optical properties of Bi:$LiNbO_3$. It has been demonstrated to result in a reliable description of defect formation energies, defect levels with respect to the band edge, and the localization of the electron distribution in many wide-band-gap semiconductors [30–37] and also in $LiNbO_3$ [30,38]. The optical properties, which mainly come from the electron transition from the occupied states to unoccupied states, could be thus more accurately described by the hybrid functional. Furthermore, the influence of Bi doping concentration on the $LiNbO_3$ optical properties is also studied in this work.

II. COMPUTATIONAL DETAILS

The present calculations employ the Vienna *ab initio* Simulation Package (VASP) [39,40] implementation of DFT in conjunction with the projector-augmented-wave (PAW) formalism [41]. Thus the Li $2s^1$, Nb $4p^6\,4d^4\,5s^1$, O $2s^2\,2p^4$, and Bi $6s^2\,6p^3$ states are treated as valence electrons. The electronic wave functions are expanded in plane waves up to a cutoff energy of 400 eV on the basis. Hexagonal supercells containing 120 atoms are used to model Bi substitutional Li (Bi_{Li}) and Nb (Bi_{Nb}) as shown in Fig. 1. Substituting one Bi atom on the Li site corresponds to a Bi doping concentration of 0.83 at.%, while Bi doping concentrations are then increased to 1.67 and 2.50 at.% by substituting two or three Bi atoms on Li sites. More than one Bi atom are placed separately from each other due to the Coulomb repulsion of the dopants with the same charges. The electron exchange and correlation (XC) functional of the general gradient approximation (GGA) with the Perdew-Burke-Ernzerhof (PBE) [42] form is used to optimize configurations with a force convergence criterion of 0.01 eV/Å, while all the energetic, electronic, and optical properties are performed by using the screened HSE06 hybrid functional. In this approach, the short-range exchange potential is calculated by mixing a fraction of the nonlocal Hartree-Fock exchange with PBE, while the long-range exchange potential and the correlation potential are calculated with the PBE functional. In our previous work, we compared the calculated lattice parameters and band gaps of $LiNbO_3$ by PBE and HSE06 functionals with experimental results as well as the calculated values by the advanced GW method [30]. We showed that the results calculated by the HSE06 functional agree well with experimental values and GW calculation values. In addition, we also studied the defect formation energies, electronic structures, and optical properties of intrinsic point defects in $LiNbO_3$ by HSE06 functional [30,38]. The results have proved that HSE06 shows well convergence of the defect formation energies and better localization of the d-electron distribution than the (semi)local GGA functional. Therefore, the HSE06 functional is reliable and accurate for calculating the structure, energetics, electronic structure, and optical properties of $LiNbO_3$. The screening and mixing parameter are fixed at 10 Å and 0.25, respectively. 4×4×4 and 2×2×2 Monkhorst-Pack [43] k-point meshes are employed to sample the Brillouin zones for PBE and HSE06 calculations, respectively.

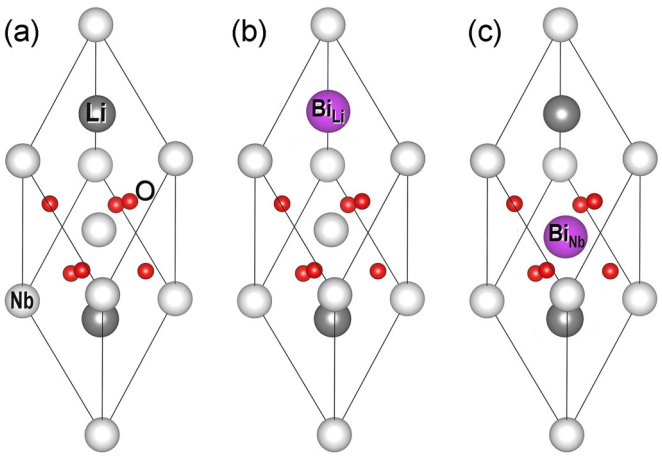

FIG. 1. Ball and stick models of pristine $LiNbO_3$ (a) and material with Bi substitutional Li (b) and Nb (c).

The defect formation energies of doping ions with q charge state dependent on the Fermi level position are calculated according to [44,45]

$$E_f(X^q) = E^{\text{total}}(X^q) - E^{\text{total}}(\text{pristine}) + \sum_i n_i\mu_i + q(E_F + E_v + \Delta V), \quad (1)$$

where $E^{\text{total}}(X^q)$ is the total energy obtained from a supercell with the doping ion X of charge state q, and E^{total}(pristine) is the total energy of the supercell without any doping ions. It is noted that the total energy E^{total} rather than the free energy G is used here since it is acceptable that the contribution from the vibrational entropy could be neglected at low temperature [46]. n_i indicate the number of atoms of species i that have been added or removed during the doping process, and μ_i are the corresponding chemical potentials. E_F is the Fermi level with respect to the pristine valence band maximum (VBM) E_v, and ΔV aligns the electrostatic potentials in the doping supercell with that in the pristine material [44].

The defect charge-state transition level $\varepsilon(q_1/q_2)$ is defined as the Fermi level position below which the defect is stable in the charge state q_1, and above which it is stable in charge state q_2 [44,47]. It is calculated as

$$\varepsilon(q_1/q_2) = \frac{E^f\left(D_i^{q_1}; E_F = 0\right) - E^f\left(D_i^{q_2}; E_F = 0\right)}{q_2 - q_1}. \quad (2)$$

The chemical potentials μ_i depend on the preparation conditions. A different choice of the reference state will modify the relative stability of the investigated doping defects. The

TABLE I. The formation enthalpy ΔH_f (in eV) of Li_2O, Nb_2O_5, and $LiNbO_3$ calculated by HSE06 as compared with the values calculated by DFT-GGA and experimental ones.

	HSE06	DFT-GGA [46]	Expt. [49]
ΔH_f ($LiNbO_3$)	−13.923	−14.433	−14.149
ΔH_f (Li_2O)	−5.975	−6.280	−6.230
ΔH_f (Nb_2O_5)	−20.211	−18.262	−19.775

thermodynamic considerations restrict the accessible range of μ_i if one requires $LiNbO_3$ stability—the stability of the ternary compound $LiNbO_3$ against decomposition into its single component constraints and its binary oxides Li_2O and Nb_2O_5 [46,48]. The details of such thermodynamic considerations could be found in Ref. [39] and in our previous work [30]. First, we compare our calculated formation enthalpies of Li_2O, Nb_2O_5, and $LiNbO_3$ by HSE06 with the values calculated by GGA [46] and the experimental values [49] as shown in Table I. It is found that the errors of ΔH_f associated with experimental results for Li_2O, Nb_2O_5, and $LiNbO_3$ are 4.1%, 2.2%, and 1.6% by HSE06 calculations, which are overall smaller than those of 0.8%, 7.7%, and 2.0% by DFT-GGA. Therefore, the HSE06 functional is more accurate than GGA in describing the energetics of the $LiNbO_3$ system. The stability range of chemical potentials of the components in $LiNbO_3$ is visualized in Fig. 2. The shaded region enclosed by BCEF indicates the $LiNbO_3$ stability range, and values outside this region lead to the precipitation of the second phases. The calculated chemical potentials of Li, Nb, and O are −2.62, −22.51, and −8.90 eV under Li-rich conditions (Li_2O reference state, line BF), while they are −3.45, −21.68, and −8.98 eV under Li-deficient conditions (Nb_2O_5 reference state, line CE). Thus we assume the Li-deficient condition in the following calculations to reappear in the experimental environment of congruent $LiNbO_3$ material. In order to repeat the experimental condition [14], the chemical potential of Bi should meet the requirement to form its oxide Bi_2O_5 as the following relation:

$$2\Delta\mu(\mathrm{Bi}) + 5\Delta\mu(\mathrm{O}) = -\Delta H_f^{\mathrm{Bi_2O_5}}. \quad (3)$$

The calculated chemical potential of Bi is −8.56 eV here.

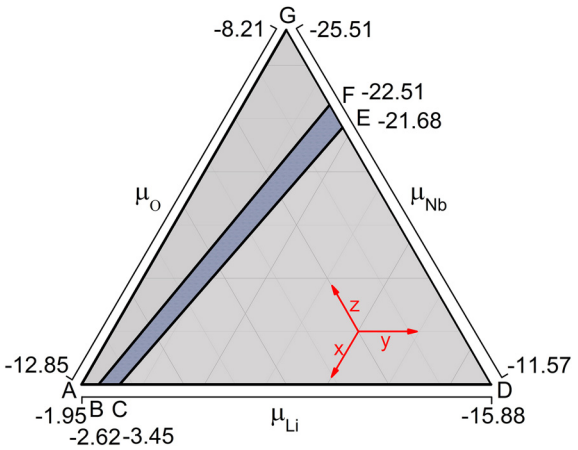

FIG. 2. Stability range of chemical potentials (in eV) of the elements in $LiNbO_3$. Lines BF and CE correspond to the Li_2O and Nb_2O_5 reference states, respectively. The shaded region enclosed between points B, C, E, and F represents the thermodynamically allowed range of the chemical potentials.

III. RESULTS AND DISCUSSION

A. Stability of Bi doping in $LiNbO_3$

Examining the relative stability of different dopants by calculating their formation energies [44,46] is widely accepted. Normally, the dopants in the lattice could trap electrons or holes and then exhibit variable charge states. For example, Bi_{Li} could exist in its charge states from +4 to 0 by capturing electrons. For Bi_{Nb} the charge states from 0 to −2 are considered here. The calculated formation energies of Bi_{Li} and Bi_{Nb} at all considered charge states as a function of Fermi energy are shown in Fig. 3, in comparison with the dominant point defects Nb_{Li} and V_{Li} in congruent $LiNbO_3$ [30,50–52]. The lowest and highest Fermi energies are assigned to be the VBM and the conduction band maximum (CBM) of the pristine structure, respectively. Therefore the range of Femi energy is set to be the calculated band gap of 4.93 eV here. The slope of the lines in the figure represents the charge state of the doping ions. Only the stable charge states for each doping type during the whole range of Fermi energy are indicated in the figure. It is noted that Bi_{Li} with a +4 charge state (Bi_{Li}^{4+}) has the lowest formation energy when the Fermi energy lies in the lower part of the electronic band gap. With the increase of Fermi energy, the most stable Bi_{Li}^{4+} transfers to Bi_{Li}^{2+} directly when $E_F = 1.8$ eV indicating that Bi_{Li}^{3+} is metastable. It is found from Fig. 3 that the thermodynamic transition level $\varepsilon(3+/2+)$ locates at 1.4 eV which is much lower than that of $\varepsilon(4+/3+)$ at 2.3 eV. This switching of the order for thermodynamic transition levels is indicative of the negative U effects [46,48], which is usually associated with a strikingly large lattice

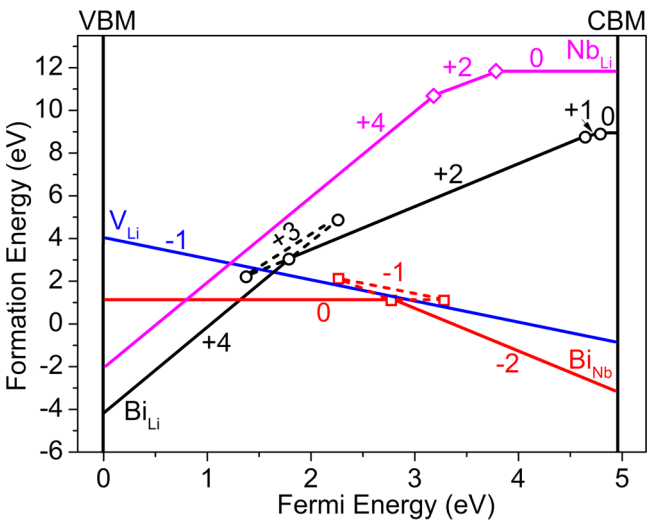

FIG. 3. Formation energies of Bi doping as well as the main intrinsic point defects Nb_{Li} and V_{Li} in $LiNbO_3$ as a function of the Fermi energy under Li-deficient condition. The Fermi energy range corresponds to the calculated fundamental band gap of 4.93 eV by HSE06 for $LiNbO_3$. The triangles enclosed by dotted lines indicate a negative U character.

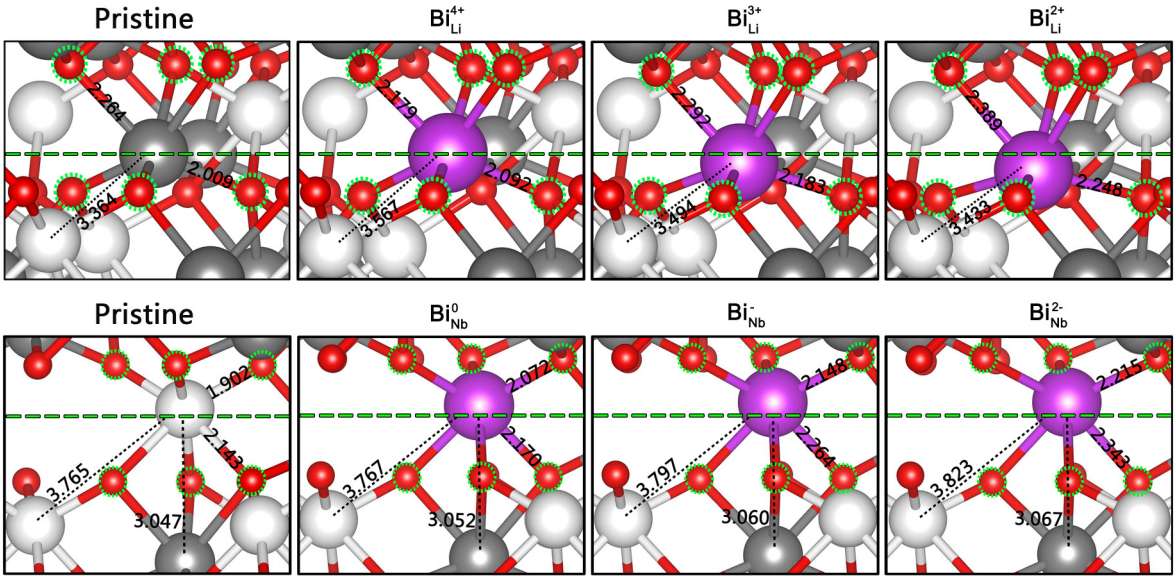

FIG. 4. Local structures of Bi_{Li} and Bi_{Nb} configurations in $LiNbO_3$. The gray, white, red, and violet balls indicate Li, Nb, O, and Bi, respectively. The distances between Bi and its neighboring O, Li, and Nb ions as well as those in the pristine material are presented in units of Å.

relaxation when capturing electrons. Further, Bi_{Li}^{2+} transfers to its +1 charge state then to its neutral state when Fermi energy lies near the CBM. It is well known that the Fermi level always lies in the middle of the fundamental band gap for the pristine system, whereas it is close to the valence and conduction bands for p-type and n-type samples, respectively. The majority of $LiNbO_3$ samples are congruent with plenty of intrinsic Li vacancies so that the Fermi level lies in the half lower part of the band gap in the realistic $LiNbO_3$ crystals. Therefore, both Bi_{Li}^{+} and Bi_{Li}^{0} are hard to form in realistic $LiNbO_3$ samples. It is noted that Bi_{Li}^{4+} transfers to the neutral Bi_{Nb} when $E_F = 1.33$ eV, indicating that with the raise of the Fermi level due to the increase of Bi doping concentration Bi could occupy the Nb site and Bi_{Nb}^{0} is energetically preferable to Bi_{Li}^{2+} when the Fermi energy lies in the middle of the band gap. The highly charged Bi_{Nb}^{2-} is only formed when the Fermi energy locates at the higher half part of the band gap. From Fig. 3 we find that the most stable Bi doping configurations Bi_{Li}^{4+} and Bi_{Nb}^{0} both have lower formation energies than those of intrinsic Nb_{Li}^{4+} and V_{Li}^{-} point defects. It is found that Bi_{Li}^{4+} transfers to the V_{Li}^{-} defect at $E_F = 1.6$ eV, and V_{Li}^{-} is energetically preferable to Bi_{Li}^{2+}, indicating the coexistence of Bi_{Li}^{2+} with intrinsic V_{Li}^{-} point defect. Overall, Bi can dope not only into the lattice of stoichiometric $LiNbO_3$ but also congruent crystals from the viewpoint of energetics. It is well accepted that $Nb_{Li}^{4+/2+}$ can act as the dominant photorefractive center in $LiNbO_3$. Both Bi substituting Li (Bi_{Li}^{4+} and Bi_{Li}^{2+}) and Nb (Bi_{Nb}^{0}) will locate apart from Nb_{Li}^{4+} due to the large Coulomb repulsion of the same highly positive charges they carried. Therefore, the interaction of Bi dopants with $Nb_{Li}^{4+/2+}$ could be ignored when investigating the Bi-induced electronic and photorefractive properties in the following parts.

In order to better understand the doping-induced lattice relaxation by capturing electrons, we have investigated the local structures of Bi substitutional Li: Bi_{Li}^{4+}, Bi_{Li}^{3+}, Bi_{Li}^{2+}, presented in Fig. 4. Distinctly, Bi substituting Li leads to quite slight local distortion of its neighboring oxygen octahedron and niobium: when a Li ion is replaced by a Bi^{5+} ($6s^0$) ion to form Bi_{Li}^{4+}, the distance between Bi and the three nearest-neighboring O along the z direction (O_{up}) is shortened by 3.54% as compared to the pristine crystal while the distance between Bi and the three nearest-neighboring O against the z direction (O_{down}) is elongated by 3.98%. It is obviously due to the movement of the Bi ion along the z direction as compared to the normal Li ion. Interestingly, as capturing one electron, the local lattice suffers large relaxation: the captured electron prefers to go where there is more free space, namely between Bi and its neighboring O_{up} atoms due to the ferroelectric distortion, and pushes the Bi_{Li}^{3+} center toward the opposite direction of the z axis due to the Coulomb repulsion of the captured electron with the electrons around O_{up} atoms. It is also observed from Fig. 4 that the distance between Bi and the three O_{down} atoms is also increased in spite of Bi movement against the z direction. This phenomenon illustrates that the three O_{down} atoms move outward accompanied by the movement of the Bi_{Li}^{3+} center. The direct observation is that the angle of O_{down}-Bi-O_{down} is increased from 107.1° in Bi_{Li}^{4+} to 112.1° in Bi_{Li}^{3+}. If Bi_{Li}^{3+} further captured another electron, the two captured electrons, acting as a lone electron pair (see Fig. 5), would also fill in the space between Bi and its neighboring O_{up} atoms, which further repulses the Bi_{Li}^{2+} center to the opposite direction of the z axis due to the increased Coulomb repulsion. Also, the three O_{down} atoms further move outward and enlarge the angle of O_{down}-Bi-O_{down} to 115.2° in Bi_{Li}^{2+}. The initial symmetry breaking is due to the covalent bonding of Bi and O_{down} (see Fig. 6), as in the case of Nb in the pristine material. However, the symmetry breaking for Bi_{Li}^{4+} is slightly smaller because the radius of Bi^{5+} (76 pm) is slightly larger than Nb^{5+} (68 pm). It is noted that the energy gain of Bi_{Li}^{3+} by large lattice relaxation could not offset the energy drop of Bi_{Li}^{2+} due to the lone electron pair occupation, exhibiting the negative U effect shown in Fig. 3.

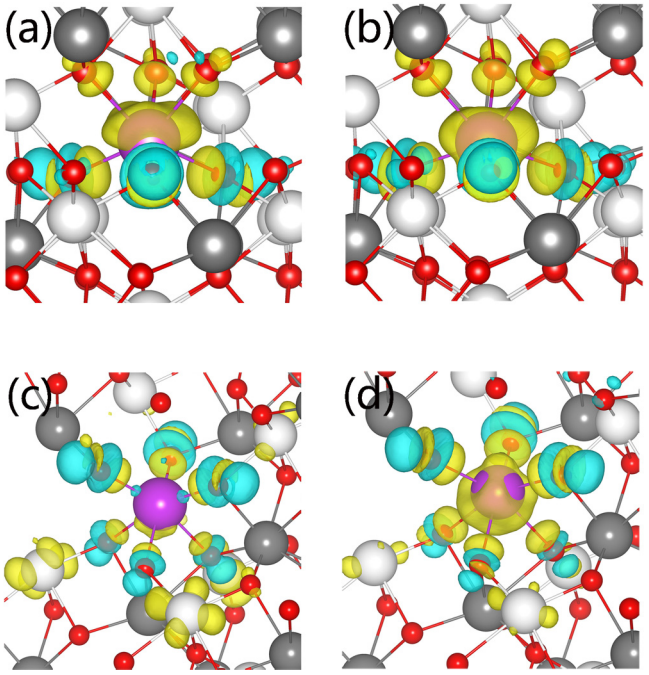

FIG. 5. Electronic charge difference maps of (a) Bi_{Li}^{4+} $(6s^0)$ − Bi_{Li}^{3+} $(6s^1)$, (b) Bi_{Li}^{3+} $(6s^1)$ − Bi_{Li}^{2+} $(6s^2)$, (c) Bi_{Nb}^{0} $(6s^0)$ − Bi_{Nb}^{-} $(6s^1)$, and (d) Bi_{Nb}^{-} $(6s^1)$ − Bi_{Nb}^{2-} $(6s^2)$. Blue and yellow regions represent electron depletion and accumulation, respectively.

A similar rule of atomic movements has been found for the case of Bi substituting Nb. For Bi_{Nb}^{0}, the distance of Bi-O_{up} is elongated by 8.95% and that of Bi-O_{down} is elongated by 1.38% as compared to the pristine crystal (Fig. 4). It indicates that Bi substituting Nb leads to the large expanding of the Nb-O octahedron. It is known that the ferroelectric polarization along the z direction leaves a large space between Nb and O_{down} atoms in pristine $LiNbO_3$. Therefore, when Bi_{Nb}^{0} captures two electrons, the lone electron pair goes to the space between Nb and O_{down} atoms, and pushes the Bi_{Nb}^{2-} center moving along the z direction, which is opposite that in Bi_{Li}. The large Coulomb repulsion between electrons also leads to the outward movement of O_{down} atoms and thus large energy gain that is responsible for the charge state transfer from 0 to −2 directly (negative U effect).

It is noted from Fig. 3 that when the Fermi energy rises up to 0.5 eV, the formation energy of Nb_{Li}^{4+} becomes positive, indicating that the further generation of the antisite defects is not energetically preferable anymore. In this case, Bi is still favored to incorporate into the Li site due to the negative formation energies. In order to further examine the Bi preferred substitution site of Nb_{Li} and the normal Li site, we define the transfer energy $E_{B\to A}^{X}$ of moving a single X atom from a B site to an A site according to

$$E_{B\to A}^{X} = E^{X}(A) - E^{X}(B) + E_{ant}(B), \quad (4)$$

$$E_{ant}^{xc} = E_{ant}(B) + E_{ant}(A), \quad (5)$$

$$\tilde{E}_{B\to A}^{X} = E_{B\to A}^{X} / E_{ant}^{xc}, \quad (6)$$

where $E^{X}(A)$ and $E^{X}(B)$ are the substitution energies of the X atom on the A and B sublattices, respectively. $E_{ant}(A)$ and $E_{ant}(B)$ are the energies of the partial antisite defects on the A and B sublattices. The negative value of $E_{B\to A}^{X}$ normally indicates a strong A-site preference of X substitution. Considering that it simply allows one to describe the site substitution behavior on two kinds of completely different sublattices in terms of a single parameter $E_{B\to A}^{X}$ in Eq. (4), we normalize $E_{B\to A}^{X}$ by the energy of forming an exchange antisite defect E_{ant}^{xc} and then get another parameter $\tilde{E}_{B\to A}^{X}$ [53]. The simple classification is as follows [54,55]:

$$\begin{aligned} \tilde{E}_{B\to A}^{X} &< 0 \quad \text{(strong A − site preference)}, \\ \tilde{E}_{B\to A}^{X} &> 1 \quad \text{(strong B − site preference)}, \\ 0 < \tilde{E}_{B\to A}^{X} &< 0.5 \quad \text{(weak A − site preference)}, \\ 0.5 < \tilde{E}_{B\to A}^{X} &< 1 \quad \text{(weak B − site preference)}. \end{aligned} \quad (7)$$

We construct a 120-atom supercell containing an isolated Nb_{Li} [treated as the A site in Eq. (4)] and a normal Li [treated as the B site in Eq. (4)], and then calculate the transfer energy of Bi moving from the normal Li site to the Nb_{Li} site. The calculated results show a negative value of −0.18 eV for transfer energy $E_{Li\to Nb_{Li}}^{Bi}$ and a small value of 0.44 eV for $\tilde{E}_{Li\to Nb_{Li}}^{Bi}$, indicating the weak site preference of the Nb_{Li} site with respect to the normal Li site for Bi substitution. It should be noted that the so-called "weak" is defined directing at two different sublattices instead of two sites in the same sublattice. Here, for

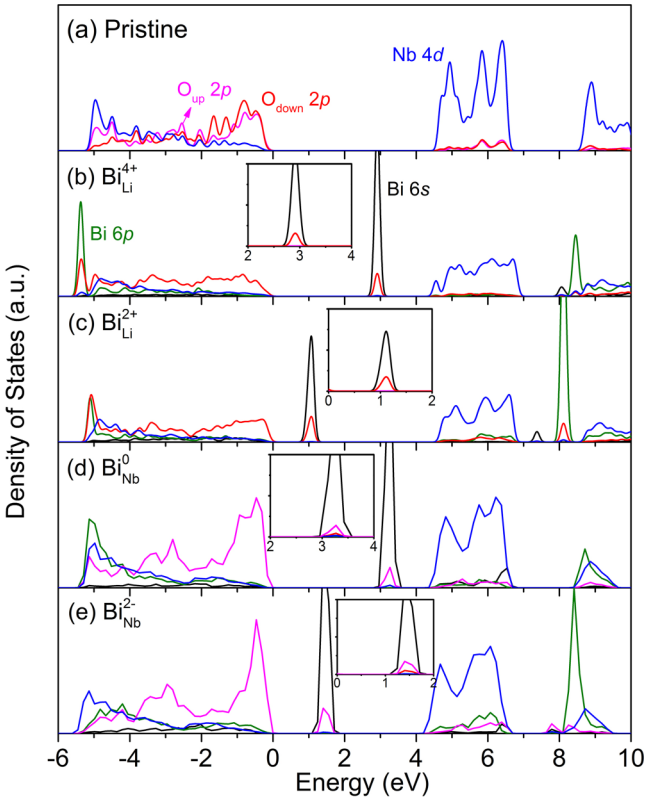

FIG. 6. The partial density of states (PDOS) of pristine $LiNbO_3$ and material with Bi_{Li}^{4+}, Bi_{Li}^{2+}, Bi_{Nb}^{0}, and Bi_{Nb}^{2-}. The dominant contributions of single atomic states including Bi $6s$, Bi $6p$, O_{up} $2p$, O_{down} $2p$, and Nb $4d$ are shown, and in the insets we show the amplified region of impurity states in the band gap with the comparison of the contribution of O_{up} $2p$ and O_{down} $2p$ states.

the case of Nb_{Li} and normal Li in the same sublattice, the calculated value of 0.44 eV for $\tilde{E}^{Bi}_{Li\rightarrow Nb_{Li}}$ could sufficiently illustrate the Nb_{Li} site preference of Bi occupation.

B. Bi impurity states and photorefractive center

In order to deeply understand the effect of Bi doping and its lone electron pair on the electronic structures of $LiNbO_3$, we have calculated the partial density of states (PDOS) of Bi_{Li} and Bi_{Nb} (see Fig. 6). It is seen from Fig. 6(b) that the formation of the most stable Bi_{Li}^{4+} ($6s^0$) introduces one $6p$ occupied state at -5.2 eV in the valence band (VB) that strongly mixes with O_{down} $2p$ states. It also introduces three empty states near the CB: two $6p$ states locating at the higher energy part of CB ($\sim$8.5 eV), and one $6s$ state locating at 2.88 eV in the band gap. By capturing two electrons simultaneously, the $6s^0$ impurity state is full-filled as the $6s^2$ electronic configuration, and the impurity state of Bi_{Li}^{2+} becomes 1.84 eV lower than that of Bi_{Li}^{4+}. Such downshift of the impurity state is partly arising from the electron occupation and also comes from the large local lattice distortion due to the Bi lone electron pair. We examine the charge distribution caused by the capture of the lone electron pair by plotting the electronic charge difference image between Bi_{Li}^{4+} and Bi_{Li}^{2+} in Fig. 5. We can clearly find that the Bi $6s^2$ lone electron pair is strongly localized in the space between Bi and O_{up} atoms. Such distribution repulses Bi moving against the z direction, and leads to the strong bonding of Bi $6s$ and O_{down} $2p$ states. Further movement of O_{up} atoms comes from the increased Coulomb repulsion between electrons that largely reduce the interaction between Bi $6s$ and O_{up} $2p$ states. These phenomena could be proved by the bonding orbital of the impurity state shown in the insets of PDOS in Figs. 6(b) and 6(c). This image confirms what we inferred from the local distortion by Bi substituting Li in the last section.

The two electrons captured by the acceptor Bi_{Li}^{4+} from the VB strongly localized around the Bi_{Li} center as the lone electron pair. The spherical and localized character of the $6s^2$ lone electron pair leads to the electron trapping at the defect center and the local distortion only referred to the first-next-neighboring atomic shell. Therefore, Bi_{Li}^{2+} could act as small bound electron polaron. This image is quite different from Nb_{Li}^{2+}, which we could treat as a Nb_{Li}^{3+}-Nb_{Nb}^{3+} ($4d^1$-$4d^1$) bipolaron [20]. The small polarons introduced by Bi doping could act as a $Bi_{Li}^{4+/2+}$ photorefractive center, which contributes to the photorefractive effect of $LiNbO_3$. It is noted that the lone electron pair is of great importance to the stability of the $Bi_{Li}^{4+/2+}$ photorefractive center. The fully occupied Bi $6s$ impurity state of Bi_{Li}^{2+} is as deep as 1.04 eV, which could reduce the recombination of the electrons in the impurity state with the holes in the VB. On the other hand, Bi doping could not affect the photorefractive properties of $LiNbO_3$ not only by introducing a new $Bi_{Li}^{4+/2+}$ photorefractive center but also by reducing the intrinsic $Nb_{Li}^{4+/2+}$ photorefractive center in $LiNbO_3$. As we discussed in the last section, Bi prefers to first substitute antisite Nb_{Li} and then normal Li sites. This indicates that with the increase of the number of $Bi_{Li}^{4+/2+}$ photorefractive centers, the number of intrinsic $Nb_{Li}^{4+/2+}$ photorefractive centers will be reduced until disappearing. Nb_{Li}^{4+} and Bi_{Li}^{4+} could act as isolated defects due to the absolutely large positive charge they carried, and the interaction of their electronic properties, including the electron distribution and the character of impurity state, could thus be ignored. It is known that the physical phenomena underlying photorefractivity are commonly described by photoexcitation of electrons from the donor centers into the CB [56]. The photorefractive properties of Bi:$LiNbO_3$ therefore refer to the photoexcitation of electrons between at least two photorefractive centers ($Nb_{Li}^{4+/2+}$ and $Bi_{Li}^{4+/2+}$), exhibiting complicated photorefractive properties. For example, the photoexcited electron from Bi_{Li}^{2+} could drift into the CB and then be trapped by Nb_{Li}^{4+}. From this point, we can infer that Bi doping concentration could change the photorefractive properties of $LiNbO_3$ via affecting the excitation and trapping of electrons by controlling the species and number of photorefractive centers.

Now we turn to the electronic structure of Bi_{Nb} which exhibits a stronger lone electron pair effect. Normally, when a Nb atom with five valence electrons is replaced by a Bi atom also with five valence electrons, Bi_{Nb} is expected to be stable in the neutral state. However, due to the strong polarization characteristic of the Nb site in the $LiNbO_3$ crystal, the unstable lone electron pair of Bi is promoted to the first excited state without bonding with O $2p$ states, and thus making Bi $6s$ impurity states empty. As seen in Fig. 6(d), the $6s^0$ impurity state of Bi_{Nb}^{0} locates at 3.45 eV in the band gap. By capturing two electrons simultaneously, the $6s^0$ impurity state of Bi_{Nb}^{0} is full-filled as the $6s^2$ electronic configuration (Bi_{Nb}^{2-}) and decreased by 1.79 eV. In this process, more electrons distribute around Bi and its neighboring O atoms which could be directly observed from the electronic charge differences in Figs. 5(c) and 5(d). The electron distribution of the Bi $6s^2$ lone pair is localized at the space between the Bi and O_{down} atoms [see Fig. 5(d)] and the impurity state of Bi_{Nb}^{2-} is mainly arising from the mixing of Bi $6s$ and O_{up} $2p$ states [see Fig. 6(e)], which is consistent with what we infer according to the local distortion of Bi_{Nb}^{2-} by electron capture. Similarly to Bi_{Li}, Bi substituting Nb forms small bound electron polarons in $LiNbO_3$ that could trap electron carriers with local lattice distortion. These small polarons could act as a $Bi_{Nb}^{0/2-}$ photorefractive center that affects the photorefractive properties of $LiNbO_3$. However, as shown in the results of charge transition levels, the trapping of electrons by the Bi_{Nb} center occurs at the Fermi level in the upper part of the electronic band gap, which indicates that the $Bi_{Nb}^{0/2-}$ photorefractive center only exists in some special environment such as n-type $LiNbO_3$ samples. In Ref. [14], Zheng *et al.* inferred that there may exist a threshold near 1.0 mol% in Bi:$LiNbO_3$ corresponding to the lattice occupation change of Bi from Li site to Nb site. Referring to the lattice occupation order of other doping ions such as Mg, Fe, etc., in $LiNbO_3$ that have reported so far, we suppose that Bi could occupy the Nb site after all the Nb_{Li} antisite is substituted by Bi ions. Under this assumption, there might exist only a $Bi_{Li}^{4+/2+}$ photorefractive center or both $Bi_{Li}^{4+/2+}$ and $Bi_{Nb}^{0/2-}$ photorefractive centers in highly Bi-doped $LiNbO_3$ crystals. If the latter is true, Bi_{Li}^{2+} and Bi_{Nb}^{2-} may form a stable defect complex with charge neutrality in $LiNbO_3$. The calculated formation energy of the $Bi_{Li}^{2+} + Bi_{Nb}^{2-}$ defect pair is 5.92 eV, which is higher than that of any isolated defects in the defect pair. However, from the aspect of formation energies, Bi_{Li}^{2+} could transfer to $Bi_{Li}^{2+} + Bi_{Nb}^{2-}$ when the Fermi level moves up to 3.23 eV with the increase of Bi doping

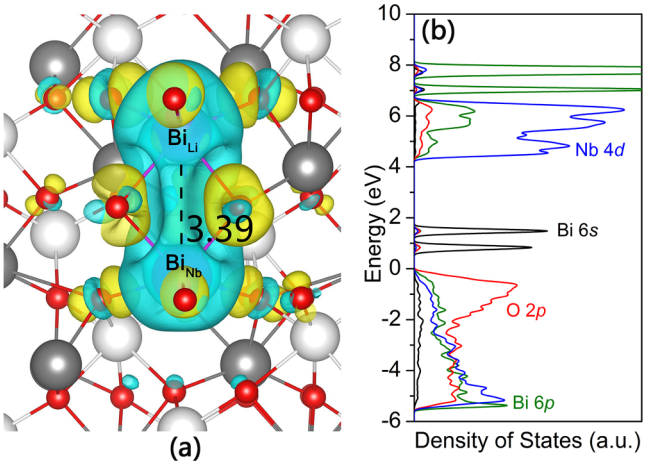

FIG. 7. (a) The isosurface of the electron density difference for the defect complex of $Bi_{Li}^{2+} + Bi_{Nb}^{2-}$. Blue and yellow regions in the upper figures represent electron depletion and accumulation, respectively. The distances between Bi_{Li} and Bi_{Nb} ions are presented in the figures in units of Å. (b) The partial density of states (PDOS) for the defect complex of $Bi_{Li}^{2+} + Bi_{Nb}^{2-}$.

concentration, namely such defect pair could exist in Bi highly doped $LiNbO_3$ samples. The distance between Bi_{Li}^{2+} and Bi_{Nb}^{2-}, which should be reduced due to the Coulomb attraction of opposite charges, is contrarily increased by 12.6% due to the location of Bi $6s^2$ lone electron pairs around the defect complex center. Besides, $Bi_{Li}^{2+} + Bi_{Nb}^{2-}$ could introduce two isolated impurity states that are occupied by the Bi $6s^2$ lone electron pair in the band gap (see Fig. 7). The two filled impurity states of the $Bi_{Li}^{2+} + Bi_{Nb}^{2-}$ cluster are downshifted with respect to the isolated state for Bi_{Li}^{2+} and Bi_{Nb}^{2-}, and more energy is needed to excite the electrons in the impurity states to the CB. However, it should be emphasized again that in the majority of cases $Bi_{Li}^{4+/2+}$ and $Nb_{Li}^{4+/2+}$ are the dominant photorefractive centers in Bi:$LiNbO_3$, and in highly Bi-doped samples, Bi substitutes the Nb site in the neutral states without the capability of hopping electrons. Generally, as the Bi lone electron pair prefers to go where there is more free space, the lone electron pair will increase the lattice distortion and thus have more obvious effect on the crystals which have intrinsic structural distortion caused by the spontaneous polarization, the second order of the Jahn-Teller effect, etc. The electronic structure and optical properties of such crystals could be modified or controlled by Bi doping or solution via the combination of the strong localized character of the lone electron pair and its induced larger structural relaxation.

C. Other optical properties of Bi:$LiNbO_3$

In this work, we also examined the Bi-doping-induced linear optical response, as well as the effect of Bi doping concentration on the optical properties of $LiNbO_3$. The imaginary parts of the dielectric function along the polarization direction $\varepsilon^{\perp}(\omega)$ for Bi_{Li} and Bi_{Nb} with their stable charge states are shown in Fig. 8. The curves corresponding to increased Bi doping concentrations (0.83, 1.67, and 2.50 at.%) are plotted in the insets. It is found that Bi_{Li}^{4+} introduces a small new peak at about 3.5 eV with respect to the pristine material,

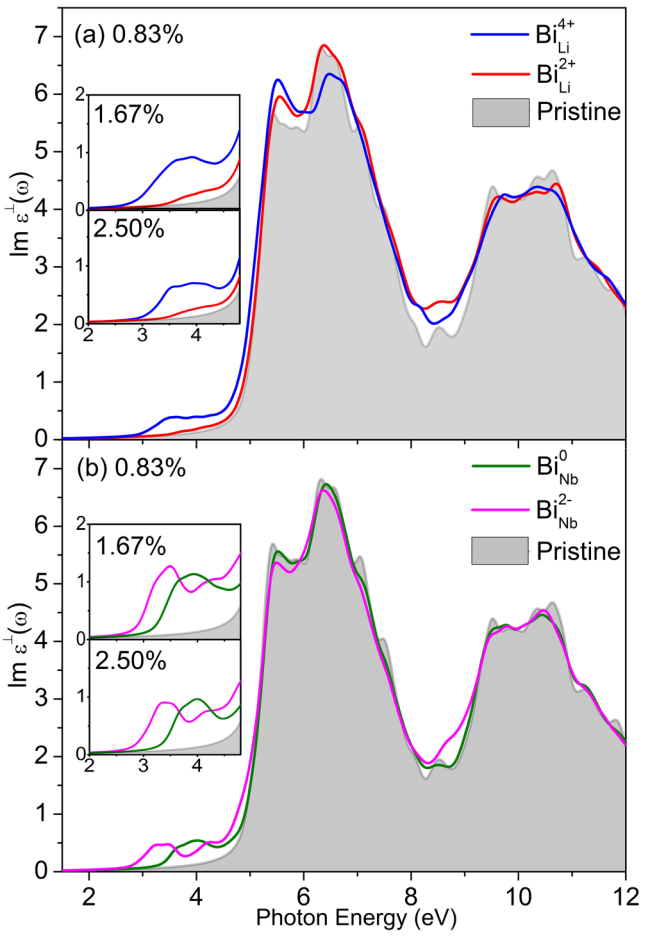

FIG. 8. Calculated ordinary optical absorption for pristine material as well as $LiNbO_3$ with Bi_{Li}^{4+} and Bi_{Li}^{2+} (a) as well as with Bi_{Nb}^{0} and Bi_{Nb}^{2-} (b) at 0.83, 1.67, and 2.50 at.% concentrations.

which is in accordance with the experimental absorption peak of Bi:$LiNbO_3$ at 330 ~ 350 nm (3.54 ~ 3.76 eV) [14]. It corresponds to the electron transition from the VBM to the empty impurity state in the band gap. Due to the downshift of Nb 4*d* states in the CBM, the main peak of Bi_{Li}^{4+} at about 5.3 eV that comes from the intrinsic electron transition from the VBM to CBM is slightly stronger than that of pristine material. Besides, absorption peaks of Bi_{Li}^{4+} between 8 and 9 eV are obviously stronger than those of pristine material due to the new electron transition from the VBM to Bi 6*p* states above 8 eV as shown in Fig. 6. When Bi_{Li}^{4+} captures two electrons to form Bi_{Li}^{2+}, the imaginary part of dielectric function exhibits some different features. One of the most obvious features is that the main absorption peak of Bi_{Li}^{2+} at 6.4 eV is stronger than that of Bi_{Li}^{4+}. This is because such absorption is composed by two parts: one is from the electron transition between the VBM and the lower part of the CB the same as that in Bi_{Li}^{4+}, while another part is from the electron transition between the impurity state in the band gap and the empty states around 7.5 eV that is absent in Bi_{Li}^{4+}. On the other hand, we cannot see the introduced absorption peak below the intrinsic absorption edge for Bi_{Li}^{2+} as in the case of Bi_{Li}^{4+} at about 3.5 eV. It is because the absorption from the electron transition between the impurity state and the low part of the CB is located at 4 ~ 6 eV,

and is mixed with the main absorption peak of the intrinsic VB-CB electron transition. It can also be found from Fig. 8(a) that the strength of the absorption peak at 3.5 eV is enhanced but its position kept unchanged with the increase of Bi_{Li}^{4+} doping concentration, indicating that there is no electronic interaction between adjacent Bi_{Li}^{4+}. From this point of view, the increase of doping concentration will not affect the stability of $Bi_{Li}^{4+/2+}$ photorefractive centers. This conclusion from the optical properties agrees well with what we get from the analysis of electronic structures. A similar effect of Bi doping concentration on the linear optical response is found for Bi_{Li}^{2+}.

Similarly to the case of Bi_{Li}, the introduction of Bi_{Nb} does not change the main feature of the imaginary part of the dielectric function of the pristine $LiNbO_3$ material [see Fig. 8(b)]. The obvious modification occurs below 5 eV: The neutral Bi_{Nb}^{0} introduces a small new peak at about 4.0 eV that corresponds to the electron transition from the VBM to the impurity state in the band gap. When Bi_{Nb}^{0} captures two electrons to form Bi_{Nb}^{2-}, the small absorption peak redshifts by 0.8 eV, and it corresponds to the electron transition from the impurity state to the conduction band. With the increase of Bi concentration, the strength of the new absorption peaks of Bi_{Nb}^{0} and Bi_{Nb}^{2-} are enhanced without any shift, confirming again that a highly Bi doped concentration could affect the photorefractive properties of $LiNbO_3$ by controlling the species and amount of photorefractive centers in the material instead of changing the stability of the $Bi_{Nb}^{0/2-}$ photorefractive center.

IV. CONCLUSION

Summarizing, hybrid DFT calculations were performed to investigate the microscopic properties of Bi:$LiNbO_3$, including the doping configurations, relative stability, electronic structure, and optical properties. In particular, the Bi lone electron pair is found to considerably influence the microscopic properties of Bi:$LiNbO_3$. From the calculation results of defect formation energies we learn that Bi_{Li}^{4+} is the most stable doping configuration when the Fermi level is at the half lower part of the band gap, and it could transfer to Bi_{Nb}^{0} with the increase of the Fermi level. Under the Li-deficient condition both Bi_{Li}^{4+} and Bi_{Nb}^{0} are energetically preferable to the intrinsic point defects Nb_{Li}^{4+} and V_{Li}^{-} in $LiNbO_3$. The stable Bi_{Li}^{4+} could trap two electrons simultaneously to form a Bi_{Li}^{2+} small bound electron polaron accompanied by a large local structural relaxation that could be described as a negative U effect. In the majority of highly Bi-doped $LiNbO_3$ samples, the neutral Bi_{Nb}^{0} does not have the ability of hopping electrons and thus could not act as a polaron. As the lone electron pair strongly localizes around the Bi center with polarization character, it leads to large distortion of the Bi-O octahedron and huge energy gain of capturing electrons that is the main contribution of the negative U effect. Furthermore, Bi doping could introduce the $Bi_{Li}^{4+}/Bi_{Li}^{2+}$ photorefractive center in $LiNbO_3$, which is deeper than the intrinsic photorefractive center $Nb_{Li}^{4+/2+}$. The electron transition between these two centers may be of benefit for the usage of the crystal in the read process of the holographic storage.

ACKNOWLEDGMENTS

We gratefully acknowledge financial support from the National Natural Science Foundation of China (Grant No. 51502158) and the Fundamental Research Funds of Shandong University (Grant No. 2015TB008).

[1] J. Ashley, M. P. Bernal, G. W. Burr, H. Coufal, H. Guenther, J. A. Hoffnagle, C. M. Jefferson, B. Marcus, R. M. Macfarlane, R. M. Shelby, and G. T. Sincerbox, IBM J. Res. Develop. **44**, 341 (2000).

[2] K. K. Wong, *Properties of Lithium Niobate, INSPEC* (IET, Stevenage, UK, 2002).

[3] V. Gopalan, V. Dierolf, and D. A. Scrymgeour, Rev. Mater. Res. **37**, 449 (2007).

[4] K. Buse, A. Adibi, and D. Psaltis, Nature (London) **393**, 665 (1998).

[5] L. Hesselink, S. S. Orlov, A. Liu, A. Akella, D. Lande, and R. R. Neurgaonkar, Science **282**, 1089 (1998).

[6] W. G. Schmidt, M. Albrecht, S. Wippermann, S. Blankenburg, E. Rauls, F. Fuchs, C. Rodl, J. Furthmuller, and A. Hermann, Phys. Rev. B **77**, 035106 (2008).

[7] A. Sanson, A. Zaltron, N. Argiolas, C. Sada, M. Bazzan, W. G. Schmidt, and S. Sanna, Phys. Rev. B **91**, 094109 (2015).

[8] R. Mouras, M. D. Fontana, P. Bourson, and A. V. Postnikov, J. Phys.: Condens. Matter. **12**, 5053 (2000).

[9] T. R. Volk, V. I. Pryalkin, and N. M. Rubinina, Opt. Lett. **15**, 996 (1990).

[10] H. Xu, A. Chernatynskiy, D. Lee, S. B. Sinnott, V. Gopalan, V. Dierolf, and S. R. Phillpot, Phys. Rev. B **82**, 184109 (2010).

[11] K. Buse, F. Jermann, and E. Kratzig, Opt. Mater. **4**, 237 (1995).

[12] W. Zhang, W. Cheng, H. Zhang, L. Geng, C. Lin, and Z. He, J. Am. Chem. Soc. **132**, 1508 (2010).

[13] C. C. Tan, A. Feteira, and D. C. Sinclair, Chem. Mater. **24**, 2247 (2012).

[14] D. Zheng, Y. Kong, S. Liu, J. Yao, L. Zhang, S. Chen, and J. Xu, AIP Adv. **5**, 017132 (2015).

[15] Y. Furukawa, K. Kitamura, A. Alexandrovski, R. K. Route, M. M. Fejer, and G. Foulon, Appl. Phys. Lett. **78**, 1970 (2001).

[16] Y. Furukawa, K. Kitamura, S. Takekawa, K. Niwa, and H. Hatano, Opt. Lett. **23**, 1892 (1998).

[17] L. Pálfalvi, J. Hebling, J. Kuhl, Á. Péter, and K. Polgár, J. Appl. Phys. **97**, 123505 (2005).

[18] R. Hammoum, M. D. Fontana, M. Gilliot, P. Bourson, and E. P. Kokanyan, Solid State Comm. **149**, 1967 (2009).

[19] F. Bridges, J. Castillo-Torres, B. Car, S. Medling, and M. Kozina, Phys. Rev. B **85**, 064107 (2012).

[20] O. F. Schirmer, M. Imlau, C. Merschjann, and B. Schoke, J. Phys.: Condens. Matter **21**, 123201 (2009).

[21] O. F. Schirmer, M. Imlau, and C. Merschjann, Phys. Rev. B **83**, 165106 (2011).

[22] D. Emin, in *Polarons* (Cambridge University Press, Cambridge, 2013), Chap. 11, pp. 95–118.

[23] I. G. Austin and N. F. Mott, Adv. Phys. **50**, 757 (2001).
[24] P. Hohenberg and W. Kohn, Phys. Rev. **136**, B864 (1964).
[25] W. Kohn and L. J. Sham, Phys. Rev. **140**, A1133 (1965).
[26] J. Hafner, J. Comput. Chem. **29**, 2044 (2008).
[27] M. Cococcioni and S. de Gironcoli, Phys. Rev. B **71**, 035105 (2005).
[28] A. Dhar and A. Mansingh, J. Appl. Phys. **68**, 5804 (1990).
[29] A. Riefer, M. Friedrich, S. Sanna, U. Gerstmann, A. Schindlmayr, and W. G. Schmidt, Phys. Rev. B **93**, 075205 (2016).
[30] Y. Li, W. G. Schmidt, and S. Sanna, Phys. Rev. B **89**, 094111 (2014).
[31] F. Oba, A. Togo, I. Tanaka, J. Paier, and G. Kresse, Phys. Rev. B **77**, 245202 (2008).
[32] P. Deák, B. Aradi, T. Frauenheim, E. Janzén, and A. Gali, Phys. Rev. B **81**, 153203 (2010).
[33] J. L. Lyons, A. Janotti, and C. G. Van de Walle, Phys. Rev. Lett. **108**, 156403 (2012).
[34] A. Janotti and C. G. Van de Walle, Phys. Status Solidi B **248**, 799 (2011).
[35] J. Paier, M. Marsman, K. Hummer, G. Kresse, I. C. Gerber, and J. G. Angyan, J. Chem. Phys. **124**, 154709 (2006).
[36] P. Agoston, K. Albe, R. M. Nieminen, and M. J. Puska, Phys. Rev. Lett. **103**, 245501 (2009).
[37] T. Shimada, T. Ueda, J. Wang, and T. Kitamura, Phys. Rev. B **87**, 174111 (2013).
[38] Y. Li, S. Sanna, and W. G. Schmidt, J. Chem. Phys. **140**, 234113 (2014).
[39] G. Kresse and J. Furthmuller, Comput. Mater. Sci. **6**, 15 (1996).
[40] G. Kresse and J. Furthmuller, Phys. Rev. B **54**, 11169 (1996).
[41] G. Kresse and D. Joubert, Phys. Rev. B **59**, 1758 (1999).
[42] J. P. Perdew, K. Burke, and M. Ernzerhof, Phys. Rev. Lett. **77**, 3865 (1996).
[43] H. J. Monkhorst and J. D. Pack, Phys. Rev. B **13**, 5188 (1976).
[44] C. G. Van de Walle and J. Neugebauer, J. Appl. Phys. **95**, 3851 (2004).
[45] S. Lany and A. Zunger, Phys. Rev. B **78**, 235104 (2008).
[46] H. Xu, D. Lee, J. He, S. B. Sinnott, V. Gopalan, V. Dierolf, and S. R. Phillpot, Phys. Rev. B **78**, 174103 (2008).
[47] C. Persson, Y. J. Zhao, S. Lany, and A. Zunger, Phys. Rev. B **72**, 035211 (2005).
[48] P. W. Anderson, Phys. Rev. Lett. **34**, 953 (1975).
[49] S. Sanna and W. G. Schmidt, Phys. Rev. B **81**, 214116 (2010).
[50] H. Donnerberg, S. M. Tomlinson, C. R. A. Catlow, and O. F. Schirmer, Phys. Rev. B **44**, 4877 (1991).
[51] N. Iyi, K. Kitamura, F. Izumi, J. K. Yamamoto, T. Hayashi, H. Asano, and S. Kimura, J. Solid State Chem. **101**, 340 (1992).
[52] Y. Li, W. G. Schmidt, and S. Sanna, Phys. Rev. B **91**, 174106 (2015).
[53] A. V. Ruban and H. L. Skriver, Phys. Rev. B **55**, 856 (1997).
[54] Z. Guoliang, D. Yongbing, S. Da, W. Jun, and S. Baode, J. Phys.: Condens. Matter. **21**, 415503 (2009).
[55] A. V. Ponomareva, E. I. Isaev, Yu. Kh. Vekilov, and I. A. Abrikosov, Phys. Rev. B **85**, 144117 (2012).
[56] P. Guenther and P. Huignard, in *Photorefractive Materials and Their Applications 2* (Springer, Berlin, 2006), Chap. 4, pp. 96–100.